

# Characterization of a miniaturized unimorph deformable mirror for high power cw-solid state lasers

Sven Verpoort, Peter Rausch, and Ulrich Wittrock  
Photonics Laboratory, Muenster University of Applied Sciences,  
Stegerwaldstrasse 39, 48565 Steinfurt, Germany,  
[verpoort@fh-muenster.de](mailto:verpoort@fh-muenster.de), [rausch@fh-muenster.de](mailto:rausch@fh-muenster.de), [wittrock@fh-muenster.de](mailto:wittrock@fh-muenster.de)

## ABSTRACT

We have developed a new type of unimorph deformable mirror for real-time intra-cavity phase control of high power cw-lasers. The approach is innovative in its combination of super-polished and pre-coated highly reflective substrates, the miniaturization of the unimorph principle, and the integration of a monolithic tip/tilt functionality. Despite the small optical aperture of only 9 mm diameter, the mirror is able to produce a stroke of several microns for low order Zernike modes, paired with a residual static root-mean-square aberration of less than 0.04  $\mu\text{m}$ .

In this paper, the characteristics of the mirror such as the influence functions, the dynamic behavior, and the power handling capability are reported. The mirror was subjected to a maximum of 490 W of laser-light at a wavelength of 1030 nm. Due to the high reflectivity of over 99.998 % the mirror is able to withstand intensities up to 1.5 MW/cm<sup>2</sup>.

**Keywords:** deformable mirror, laser, adaptive optics, bimorph, unimorph

## 1. INTRODUCTION

It has been shown that the beam quality and the efficiency of high-power solid state lasers can be enhanced by the use of deformable mirrors in order to compensate for optical aberrations. Intracavity compensation requires a deformable mirror which is capable of handling very high laser intensities. The active diameter of the deformable mirror should be a few millimeters in order to match typical fundamental mode laser beam diameters. There is a wide variety of commercially available deformable mirrors, but none of them meets all these requirements. We present a new type of unimorph deformable mirror with monolithic tip/tilt functionality that does meet all requirements.

The most prominent feature that distinguishes this mirror concept from many others is that it employs an optical glass substrate that is super-polished and furnished with a dielectric coating before the deformable mirror is assembled. This ensures that we can achieve a highly reflecting and extremely low-scattering optical surface that rivals the best passive optics.

Furthermore, our deformable mirrors use very thin substrates and pre-fabricated ceramic PZT actuators. This leads to a large stroke. Finally, our mirror concept has the added advantage that it features an integral tip-tilt functionality. All other bimorph and unimorph mirrors we know need a separate tip-tilt mirror in order to achieve any significant amount of tip-tilt correction.

## 2. MIRROR DESIGN

Figure 1 shows a cross-sectional view of our unimorph mirror design. This mirror represents a further development of our elastically mounted unimorph mirror design presented in [1, 2]. The structure is based on a laser-cut 3-arm piezoelectric disc. The disc is sandwiched between two metallic electrodes, an unstructured ground electrode on the front side and a structured back-side electrode. The electrode structuring is done by laser ablation with an ultrashort-pulse ps-

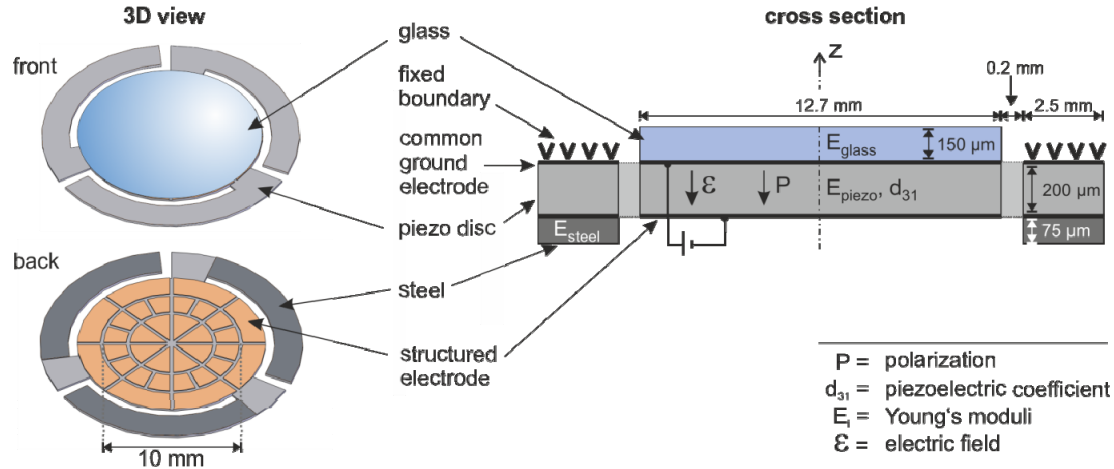


**Fig. 1:** a) Three-dimensional view of the demonstrator mirror along with the configuration of the electrode pattern, b) Corresponding cross-sectional view

laser. Three laser-cut steel segments are adhesively bonded onto the spiral arms of the piezo structure to facilitate tip/tilt actuation of the arms. The central disc of the piezo structure is adhesively bonded to a passive glass substrate. The glass substrate is a thin disc of super-polished high-quality optical glass furnished with a high-reflective dielectric coating. The ends of the three arms are bonded to the support points of an aluminum mounting ring by an electrically conductive adhesive. A detailed description of the entire assembly including the housing and the electrical periphery is given in chapter 3. The main specifications of the mirror design are listed in table 1. The mirror features a diameter of the reflective surface of 12.7 mm paired with a 35 keystone electrode pattern. In the past, we have carried out extensive numerical calculations to analyze and compare different electrode patterns with respect to the amplitude and the fidelity with which certain low-order Zernike modes can be created [3]. The optimized design features a 32-electrode keystone pattern, 24 electrodes inside the 10 mm optical aperture, and 8 electrodes forming an additional outer ring outside of the optically active area. This electrode pattern enables a high-fidelity Zernike reproduction with sufficient stroke. Three electrodes are used to actuate the arms.

The geometry parameters, e.g. layer thicknesses and diameters as well as the material selection and the electrode pattern have been optimized by means of analytical and numerical calculations. The thicknesses of the glass substrate and the piezoelectric element have been chosen to achieve a sufficient stroke while providing as much passive stiffness of the mirror as possible.

Table 1. Mirror Specifications

Attribute	Value / Description	
Diameter	total:	Ø 18.1 mm
	central disc:	Ø 12.7 mm
	clear optical aperture:	Ø 9 mm
Piezoceramic layer	material:	PIC 255
	thickness:	200 μm
	Poisson ratio:	0.36
	Young's modulus E:	62.9 GPa
	piezoelectric voltage coefficient $d_{31}$ :	$-180 \times 10^{-12}$ (m/V)
	electrode material:	screen-printed Ag, thickness 10 μm

Glass layer	material: thickness: Poisson ratio: Young's modulus E:	N-BK10 150 $\mu\text{m}$ 0.208 72 GPa
Steel layer	material: thickness: Poisson ratio: Young's modulus E:	austenitic stainless steel (X2CRNi18-9) 75 $\mu\text{m}$ 0.3 210 GPa
Reflective coating	type: <b>front side:</b> surface roughness: <b>back side:</b>	dielectric multilayer system HR ( $R > 99.998\%$ @ 1030 nm, $0^\circ$ ) < 1.5 $\text{\AA}$ RMS AR stress compensation layer
Electrode pattern	number of actuators layout	35 FEM optimized keystone pattern

### 3. FABRICATION WORKFLOW

This section describes the individual steps of the fabrication process. The workflow is depicted schematically in figure 4.

#### 3.1 Step 1: Grinding and Lapping

In a first step we characterized the initial deformation of commercially available off-the-shelf piezoelectric discs with a diameter of 20 mm and a thickness of 200  $\mu\text{m}$ . These discs were already furnished with Ag-thick-film electrodes on both sides. The surface profiles were measured with a commercial 3D stripe projection shape measurement system. The results presented in Fig. 2a show a primarily astigmatic initial deformation of the disc which are inevitably induced during the manufacturing process. In order to provide a sufficient flatness for the bonding of the glass substrate the piezoelectric discs have been ground and lapped on one side, the resulting surface shape is shown in Fig. 2b. As can be seen in the interferogram, the residual deformation exhibits a primarily spherical shape. The lapping procedure has been optimized to produce a remaining surface roughness of 4-6  $\mu\text{m}$  RMS to increase the adhesive force in the bonding step. After the lapping process the surface morphology was examined using a scanning electron microscope. The results from the microscopic evaluation show a surface roughness of 5.7  $\mu\text{m}$  which lies within the targeted range.

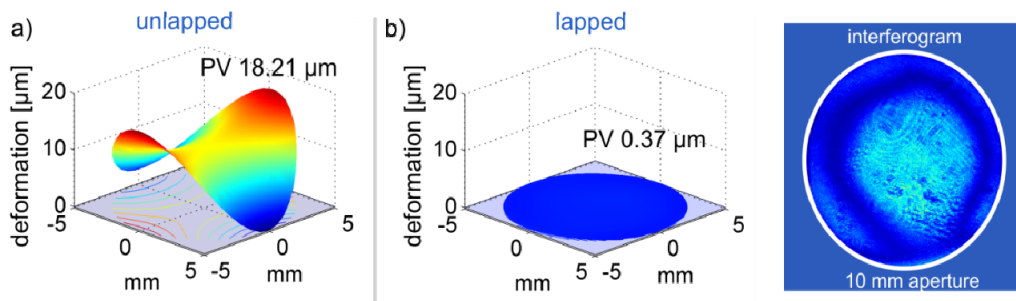


**Fig. 2:** Comparison of the surface profile of a piezoelectric disc **a)** before and **b)** after the grinding/lapping step

### 3.2 Step 2: Application of New Ground Electrode

After the lapping step, a new ground electrode was applied onto the lapped side. The electrode layer has been deposited by thermal evaporation. Aluminum was chosen as electrode material because it adheres well to the piezoceramic material and forms smooth films with small grain size. Sheet resistances near  $1550 \Omega/\text{m}^2$  are produced for thicknesses between 200 and 300 nm. The thickness of the deposited aluminum layer was measured to be approximately 220 nm.

### 3.3 Step 3: Laser Cutting of the Piezoelectric Disc

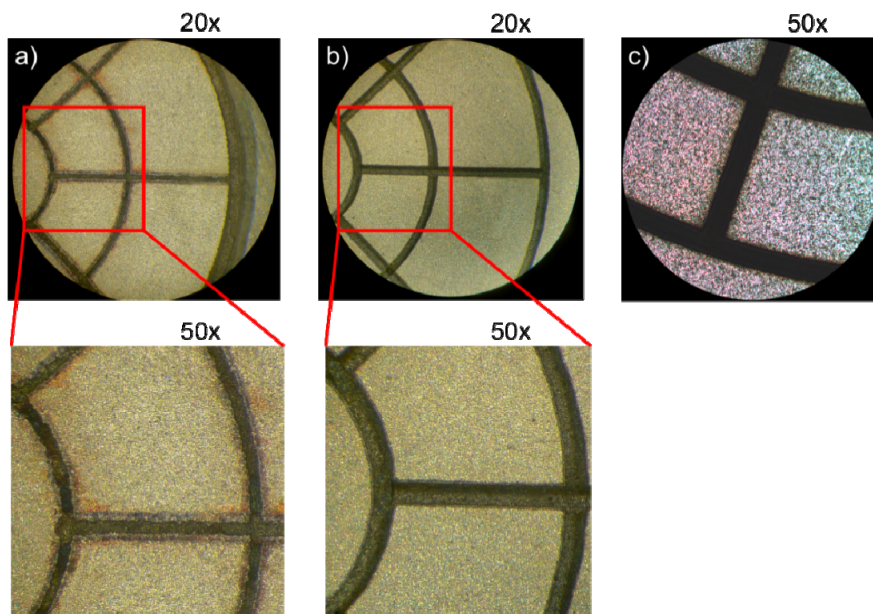
Cutting the spiral arm structure out of the piezo disc was carried out with an ultrashort-pulse ps-laser. The extremely short pulses of less than 10 picoseconds vaporize the material so quickly that no heat affected zone can be detected (“cold” materials processing).

### 3.4 Step 4: Electrode Patterning

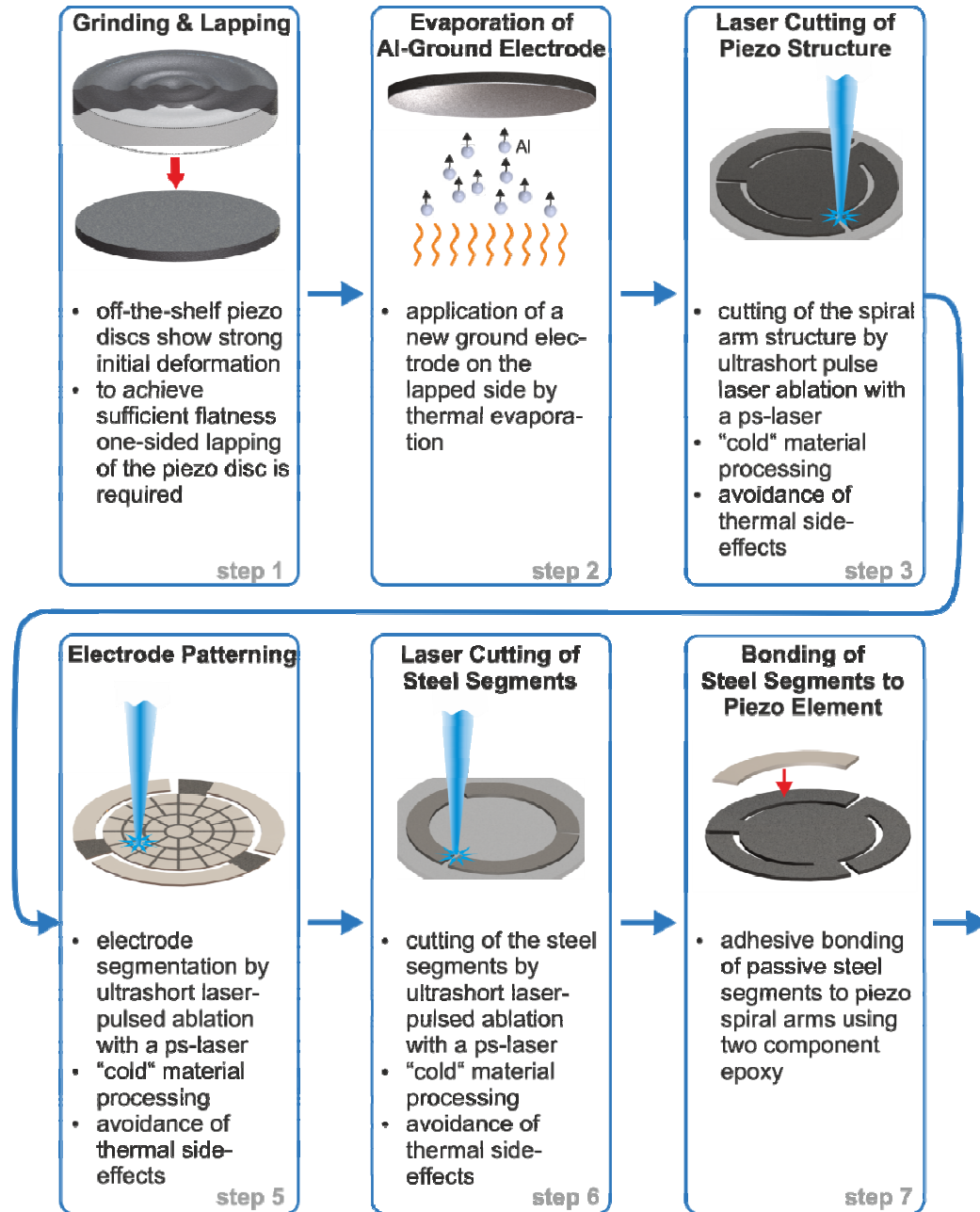
The segmentation of the back side electrode was performed by laser ablation. For this step we carried out a comparison between three different laser systems. The technical data of the investigated laser systems are given in table 2. The best results were achieved with the TruMicro ps-laser. As can be seen in Fig. 3c there is no formation of shavings, melt or debris along the laser-structured track, and no delamination of the electrode layer. The parameters of the structuring processes have been optimized to guarantee a complete cut through the electrode layer and to prevent electric breakthrough caused by irregular cutting edges with sharp features.

Table 2. Technical Data of the Investigated Laser Systems

	Rofin / Sinar Powerline RSY 90 QL	TRUMPF TruMark Station 6020	TRUMPF TruMicro 5050
Pulse duration	100 ns	15-20 ns	< 0.01 ns
Beam quality $M^2$	20	1.2	< 1.3
Repetition rate	0-25 kHz	1-120 kHz	200-800 kHz
Wavelength	1064 nm	1064 nm	1030 nm



**Fig. 3:** Comparative microscopic images of the electrode segmentation:  
**a)** Rofin-Sinar **b)** Trumpf TruMark 6020 **c)** Trumpf TruMicro 5050



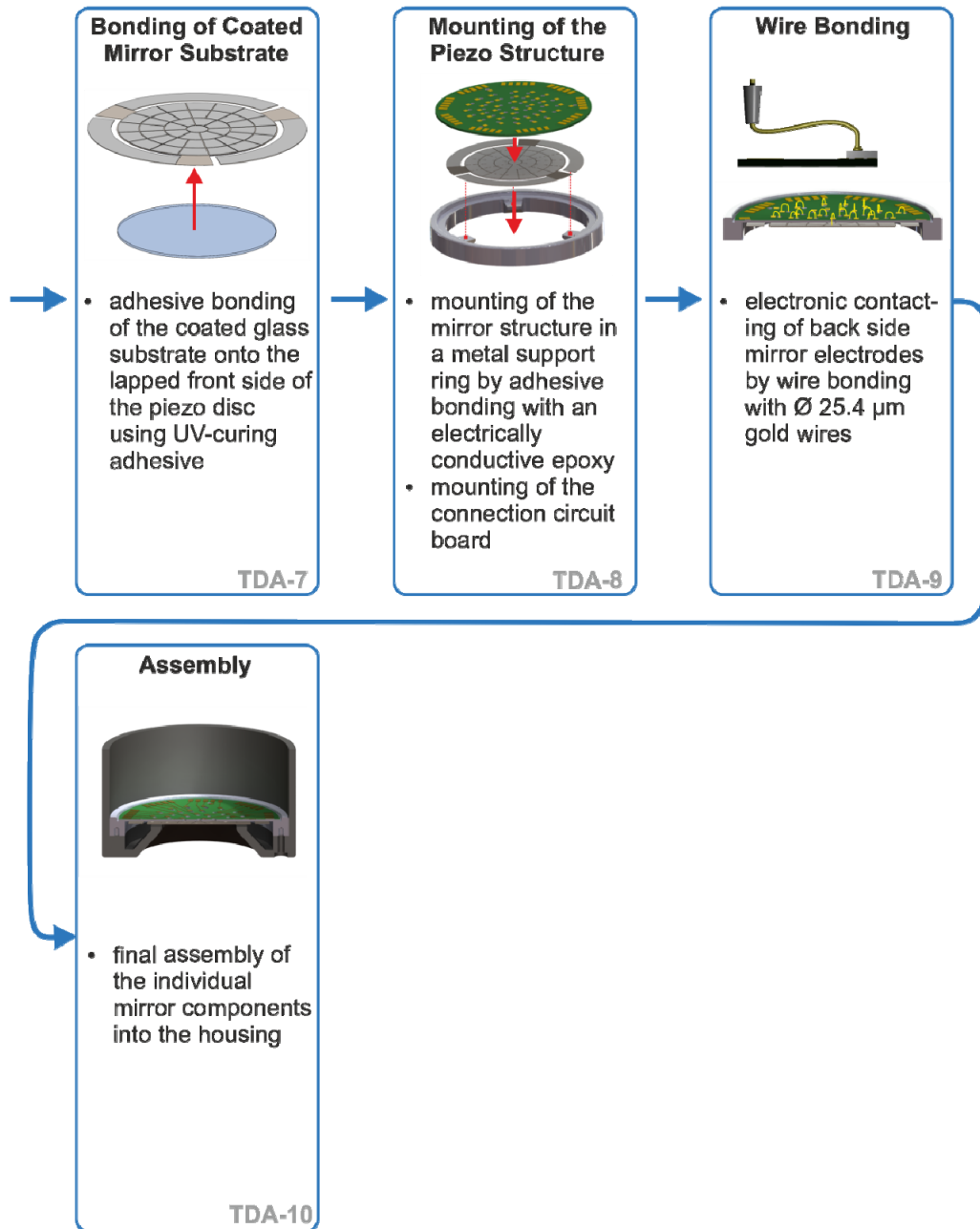


**Fig. 4:** Schematic representation of the fabrication workflow

### 3.5 Step 5: Laser Cutting of the Steel Segments

To facilitate tip/tilt actuation three steel segments are bonded to the piezoelectric element as passive layers. The elements are made from  $75 \text{ }\mu\text{m}$  thick stainless steel foil. The cutting of these segments is carried out with a 20 W fiber laser from SPI Lasers. An image of the cut steel segments is shown in Fig. 5a.

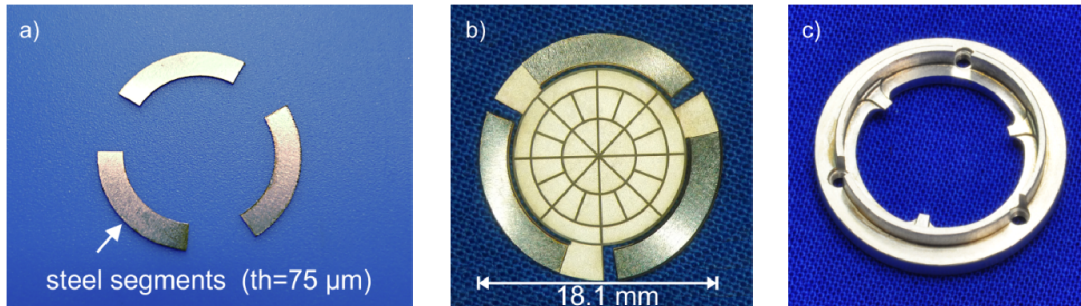


**Fig. 5:** a) laser cut steel segments, b) segments bonded to piezo element, c) mounting ring

### 3.6 Step 6: Bonding of the Steel Segments

In this step the cut steel segments are adhesively bonded onto the arms of the piezoelectric spiral arm structure. This is done using a two-component epoxy. The adhesive exhibits a good adhesion to metal and ceramic material, accompanied with very low shrinkage. Figure 5b shows the already bonded piezo structure.

### 3.7 Step 7: Bonding of the Mirror Substrate

As mentioned in the previous chapter, super-polished and dielectrically coated glass substrates were adhesively bonded to the piezo element. The substrates made from N-BK10 have a diameter of 12.7 mm and a thickness of 150 μm. The coating specifications are given in table 3. Due to its excellent surface wettability, bonding strength, and its very low curing induced stress, a UV-curing adhesive was used. An image of the coated glass substrate is shown in Fig. 6.

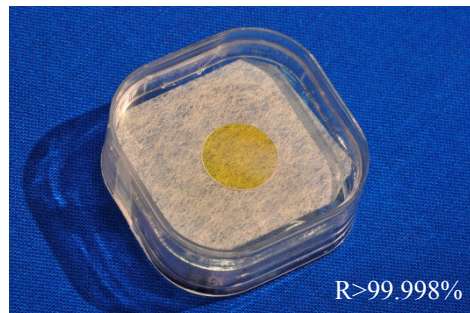


**Fig. 6:** HR-coated super-polished glass substrate

Table 3. Coated Glass Substrate Specifications

	Coated glass substrates
Coating front side	HR(0°, 1030nm) > 99.998%
Coating back side	AR(0°, 1030nm) stress compensation layer
Coating process	magnetron sputtering
Glass substrates	material: N-BK10 diameter: Ø 12.7 mm thickness: 150 μm surface roughness: < 1.5 Å RMS

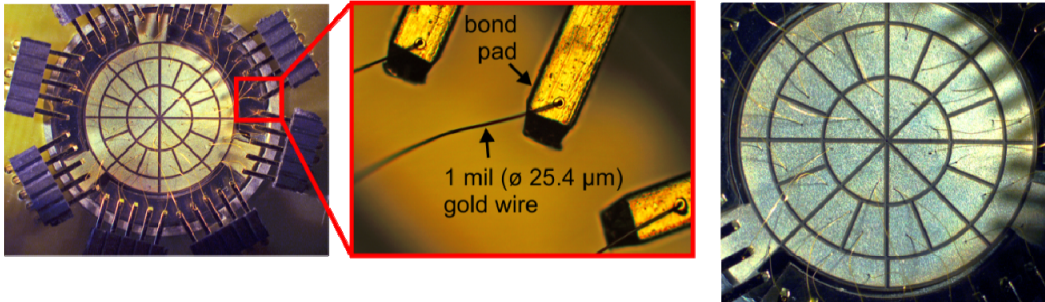


**Fig. 7:** Electrical interconnections provided by wire bonding of the back side electrodes

### 3.8 Step 8: Mounting of the Piezo Structure

The mounting of the mirror structure is done by adhesive bonding of the spiral arm ends to three fixture points of a metal support ring (see Fig. 5c). For this process step, the electrically conductive epoxy H20E from Epo-Tek is used. The bonding joints provide electric connection between the metal support ring and the mirror ground electrode.

### 3.9 Step 9: Electric Contact by Wire Bonding

Electrical connection is established by wire bonding of very thin 1 mil (25.4  $\mu\text{m}$ ) gold wires to the mirror electrodes and the connection pads. For this purpose, a commercial ultrasonic ball-wedge wire bonder from West-Bond is used. The process uses a combination of pressure and ultrasonic energy to make a weld at each end of the wire. During wire bonding, a gold ball is first formed by melting the end of the wire (which is held by a bonding tool known as a capillary) through electronic flame-off (EFO). This ball has a diameter ranging from 1.5 to 2.5 times the wire diameter. Ball size consistency, controlled by the EFO and the tail length, is critical in good bonding. The gold ball is then brought into contact with the bond pad. Adequate amounts of pressure and ultrasonic forces are then applied to the ball for a specific amount of time, forming the initial metallurgical weld between the ball and the bond. The wire is then routed to the corresponding finger of the leadframe, forming a gradual arc or "loop" between the bond pad and the leadfinger. Pressure and ultrasonic forces are applied to the wire to form the second bond (known as a wedge bond, stitch bond, or fishtail bond), this time with the leadfinger. The wire bonding machine breaks the wire in preparation for the next wire bonding cycle by clamping the wire and raising the capillary. Figure 7 shows the connected mirror electrodes after the bonding process. Wirebonding has the great advantage, compared to other techniques like soldering or glueing, that the very thin gold wires do not exert any significant force on the mirror structure. Also, the bonds are small enough such that they do not increase the local stiffness of the piezo ceramic.

### 3.10 Step 10: Final Assembly

In the last step, the connection circuit board with the embedded mirror structure is inserted in a sturdy aluminum mirror housing (see Fig. 8). The connection circuit board is plugged onto a back panel circuit board, which is attached to the housing cover. The back panel circuit board features a 40-channel connector socket.

This sequence of manufacturing steps is different from the conventional way of manufacturing deformable mirrors. Conventionally, the substrate that will later bear the reflective coating is first attached to the actuator structure. In the next step the front surface of the substrate is polished (except for membrane mirrors which are not polished but created by an etching process). Finally, the polished surface is coated with a dielectric coating. This method of producing a deformable mirror has the advantage that surface deformations that have occurred due to the manufacturing steps will be removed during the polishing process. However, the method has the serious disadvantage that the already assembled mirror needs to be polished, cleaned, and placed in a vacuum chamber to produce the dielectric coating. Dielectric coatings with very high reflectivity and low scattering require extremely well-polished substrates, very careful cleaning of the substrate before coating, and special coating techniques such as magnetron sputtering and ion beam sputtering. Coating vendors usually require that they do all three processes (polishing, cleaning, coating) themselves and on their



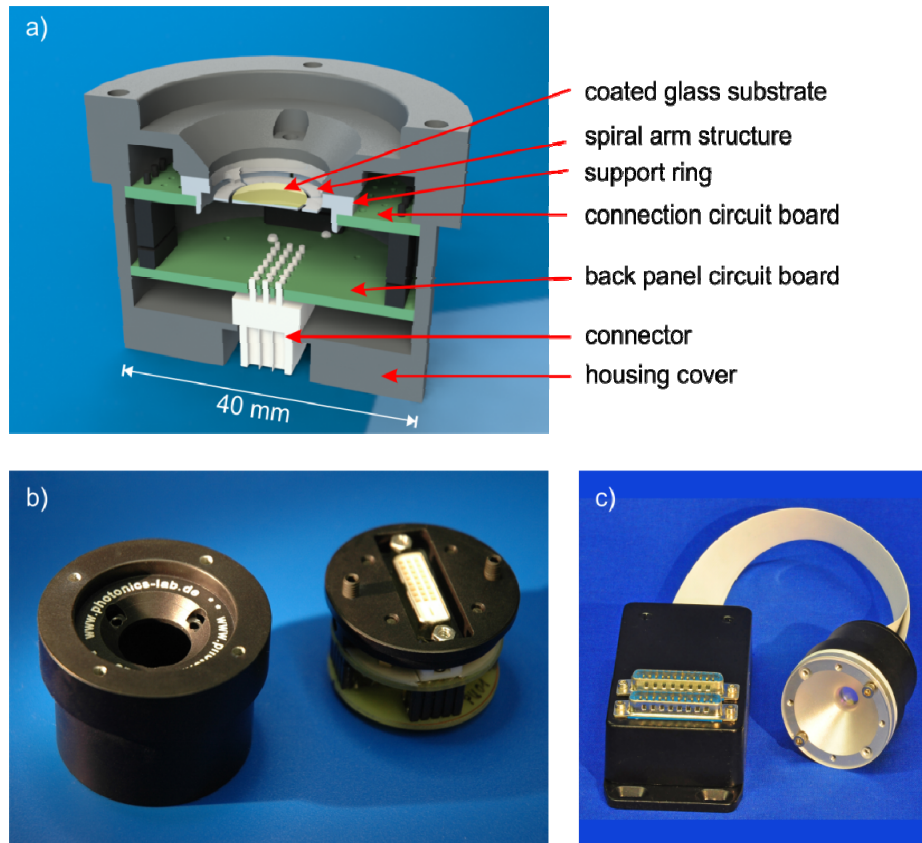


**Fig. 8:** a) cross-sectional view of the assembled mirror prototype, b) mirror housing, c) assembled mirror with adapter box

own glass substrates in order to guarantee the quality of the coating. These processes are usually hard to be done when the mirror is already assembled. Additionally, when using very thin laminates to achieve high stroke, a sputtered coating leads to stress-induced deformations. In our mirror, this is compensated by a stress compensation layer on the back side of the glass substrate, which cannot be done when the mirror substrate is already bonded. For the manufacture of such high-quality coatings a substrate with a surface roughness of  $1 \text{ \AA}$  is required which can only be achieved by super-polished optical glass. Diamond-turned surfaces which are used in other mirror designs have one to two orders of magnitude larger surface roughness. Piezoelectric materials themselves and many substrate materials other than high-quality optical glass cannot be super-polished to a surface roughness of  $1 \text{ \AA}$ . Silicon membranes cannot be cleaned because they have a thickness of only a few micrometers. In our tests, the membranes also were regularly destroyed during the coating process due to the high tension of the coating. Only thermally evaporated (electron-beam heated) coatings with a low number of layers could be applied but lacked the requirement for low scattering and very high reflectivity.

Polishing the mirror substrate before mounting it to the actuator structure requires that the mounting process does not introduce any stresses. Such stresses would result in deformation of the assembled mirror. This requires a special mounting procedure which we have established.

To summarize, our design allows to fabricate deformable mirrors from high-quality, super-polished discs of optical glass that are coated with sputtered dielectric coatings. This way, a reflectivity larger than 99.99% can be guaranteed. Even reflectivities larger than 99.999% have been achieved on super-polished glass substrates and measured by cavity ring-down spectroscopy.

Any light that is transmitted by the coating is absorbed by the (generally piezoelectric) actuator and will heat up the deformable mirror. This leads to thermal deformation or even destruction of the mirror. Deformable mirrors are much more sensitive in this respect than conventional mirrors. In a conventional mirror, light that is transmitted by the coating is usually also transmitted by the mirror substrate. Thus it does not heat up the mirror. Even if light is absorbed in a conventional mirror it leads to much less deformation because these mirrors have much thicker substrates than deformable mirrors.

## 4. EXPERIMENTAL CHARACTERIZATION

### 4.1 Surface Profile Measurement

The surface shapes were measured using a phase-stepping interferometer. This system allows a very precise wavefront measurement with a resolution up to  $\lambda/100$ . The barplot in Fig. 9 shows the achievable Zernike amplitudes of our unimorph mirror design. The evaluation of the surface deformation has been carried out across the central 9 mm diameter optical aperture. The Zernike amplitudes have been evaluated under the condition that the residual rms wavefront error  $\sigma_{rms}$  maintains the Maréchal criterion  $\lambda / 14$  for  $\lambda = 1064$  nm ensuring diffraction-limited imaging and that the actuator voltages stay inside the maximum allowed voltage range. This voltage range (-100 V to +100 V) is determined by electric field breakthrough and reverse poling of the piezoelectric material.

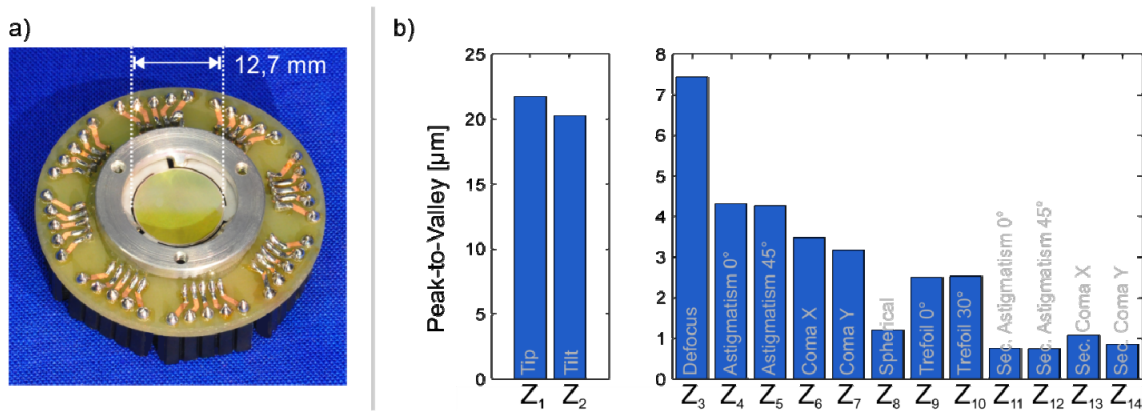


Fig. 9: a) prototype mirror, b) measured peak-to-valley Zernike amplitudes

### 4.2 Dynamic Behavior

Critical characteristics of piezoelectric materials are hysteresis and non-linearity. The predictability of the mirror response to applied voltages is essential for an accurate open-loop and feed-forward operation. Over the full working range, the PIC 255 piezoelectric material exhibits approximately 14% hysteresis. The linearity of the mirror can be improved by means of an analytical compensation based on an inverse Preisach hysteresis model. It could be shown experimentally that the hysteresis of a piezo actuator can be reduced from 20% to about 6% [4]. In closed-loop operation, any non-linearity will be corrected automatically, albeit associated with some loss of bandwidth.

A high temporal correction bandwidth of the deformable mirror can be achieved by providing high mechanical resonance frequencies and at the same time sufficiently high structural damping. Additionally, electronic damping can be employed by smart control systems where the electrode actuation counteracts the occurrence of resonance oscillations. The dynamic behavior of the mirror has been assessed by means of resonance frequency analysis. Figure 10 shows the results of a frequency response analysis. The first natural frequency occurs at  $f_1 = 1500$  Hz and corresponds to a piston-like

mode shape. The next two modes are tilting modes. All of the three lowest modes shown in Fig. 10 are actually caused by bending of the three support arms. These modes could easily be moved to frequencies that are twice as high by increasing the stiffness of the three support arms. This would only entail a reduction of the tip/tilt amplitude. The resonance frequencies of the mirror without the support arms are well above 5 kHz. The deformable mirror therefore offers an accessible bandwidth of 500 Hz.

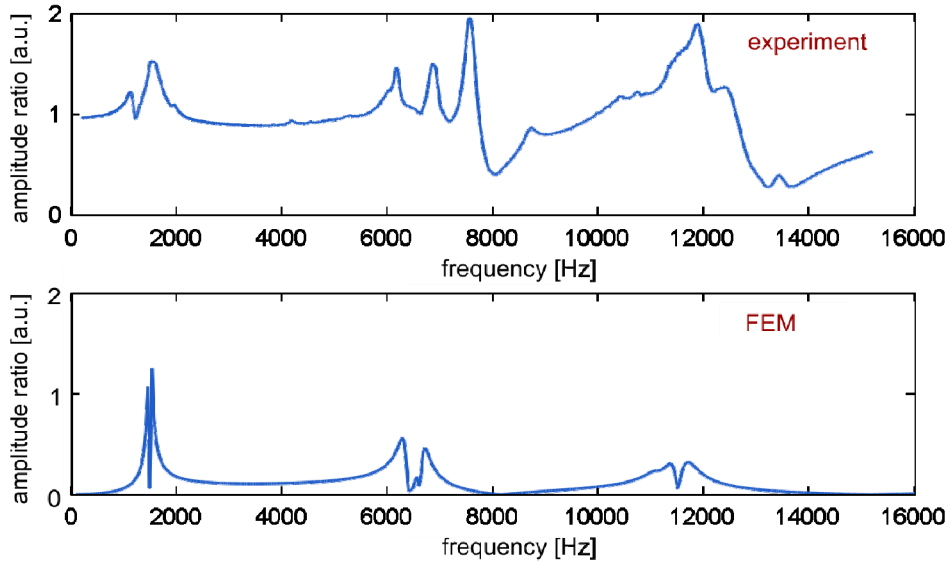


Fig. 10: Comparison of the measured and calculated resonance frequency behavior

### 4.3 Power Handling Capability

To assess the mirror’s power handling capability we have illuminated the mirror with a 490 W laser beam of a thin-disc laser system with a wavelength of 1030 nm. The beam with a beam quality of  $M^2=20$  has been focused down to a spot size of only 101  $\mu\text{m}$  leading to a power density in the focal spot of approximately 1.5  $\text{MW}/\text{cm}^2$  (see Fig. 11). We have recorded the temperature of the mirror structure over a period of 30 minutes. During this period the temperature increase stayed below 2°C. The temperature change within the first four minutes is shown in Fig. 12. During and after illumination no thermally induced deformation could be detected.

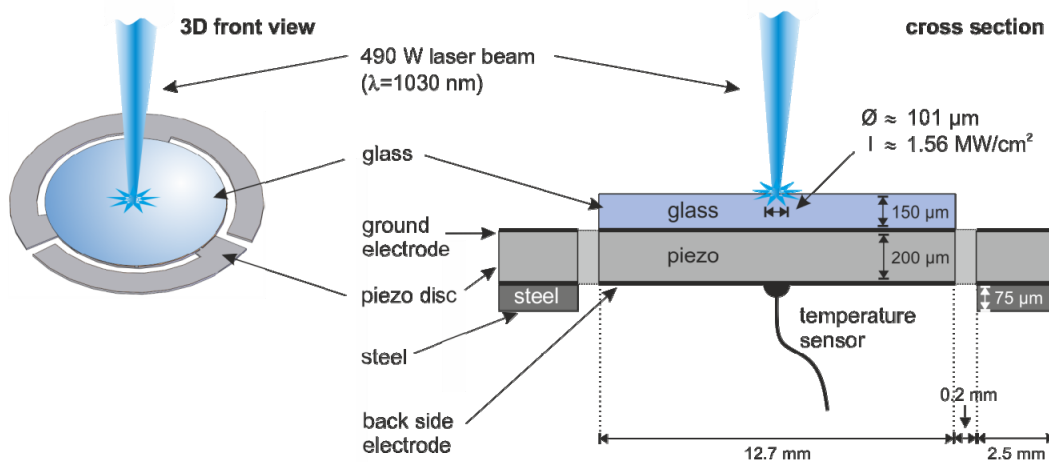
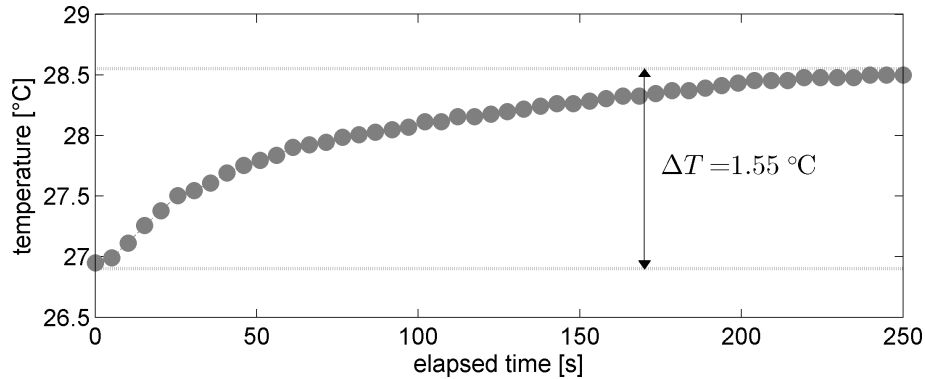


Fig. 11: Experimental setup for measuring the power handling capability



**Fig. 12:** Measured temperature increase of the mirror structure under illumination with a 490 W laser

## 5. CONCLUSION

We have presented a concept for a unimorph deformable mirror suitable for use in high power laser resonators. Experimental results show that the mirror can correct low order aberrations with high stroke and at the same time good surface fidelity. This is made possible by using high-quality precoated substrates which allow a very thin laminate thickness. The novel spiral arms enable an additional tip/tilt correction which simplifies resonator alignment.

## 6. ACKNOWLEDGMENTS

The authors gratefully acknowledge support for the work presented by the German Ministry for Education and Research (Bundesministerium für Bildung und Forschung, BMBF) under contract 1726X09 and by Thorlabs GmbH.

## REFERENCES

- [1] Verpoort, S., Welp, P. and U. Wittrock, "Novel unimorph deformable mirror for solid state laser resonators," in MEMS Adaptive Optics III (part of Photonics West 2009), Proc. SPIE 7209, 7209-22 (2009)
- [2] Verpoort, S. and Wittrock, U., "Miniaturized adaptive mirror for solid state laser resonators," in Proceedings of the 7<sup>th</sup> International Workshop on Adaptive Optics for Industry and Medicine, Russia (2009)
- [3] Verpoort, S. and Wittrock, U., "Actuator patterns for unimorph and bimorph deformable mirrors," Appl. Opt. 49, G37-G46 (2010)
- [4] Song, H., Fraanje, R., Schitter, G., Verhaegen, M. and Vdovin, G., "Hysteresis compensation for a piezo deformable mirror," in Adaptive Optics for Industry and Medicine, Proceedings of the 6<sup>th</sup> international Workshop, C. Dainty ed., 112-117 (Imperial College Press, 2008)